Heliyon 10 (2024) e37426

Contents lists available at ScienceDirect

Heliyon

journal homepage: www.cell.com/heliyon

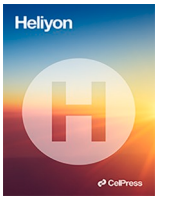

Research article

Soil moisture inversion based on multiple drought indices and RBFNN: A case study of northern Hebei Province

Xiao Wang [a], Haixin Liu [a,*], Zhenyu Sun [a], Xiaoqing Han [b]

[a] College of Mining and Geomatics, Hebei University of Engineering, Handan, China
[b] Jizhong Energy Fengfeng Group Company Limited, Gaokai District, Handan, China

ARTICLE INFO

Keywords:
Drought index
MODIS
Radial basis function neural network
Remote sensing

ABSTRACT

Drought has a significant impact on crop growth and productivity, highlighting the critical need for precise and timely soil moisture estimation to mitigate agricultural losses. This study focuses on soil moisture retrieval in northern Hebei Province during July 2012, utilizing eight widely employed remote sensing drought indices derived from MODIS satellite data. These indices were cross-referenced with measured soil moisture levels for analysis. Based on their correlation coefficients, a composite remote sensing drought index set comprising six indices was identified. Furthermore, a radial basis function neural network (RBFNN) was employed to estimate soil relative humidity. The accuracy evaluation of the soil moisture estimation model, which integrates multiple remote sensing drought indices and the RBFNN, demonstrated clear superiority over models relying on single drought indices. The model achieved an average estimation accuracy of 87.54 % for soil relative humidity at a depth of 10 cm (SM10) and 87.36 % for a 20 cm depth (SM20). The root mean square errors (RMSE) for the test sets were 0.093 and 0.092, respectively. Validation results for July 2013 indicated that the inversion accurately reflected the actual soil moisture conditions, effectively capturing dynamic moisture changes. These results fully verify the reliability and practicability of the model. These findings introduce a novel approach to local agricultural soil moisture estimation, with significant implications for enhancing agricultural water resource management and decision-making processes.

1. Introduction

Drought is a significant global natural disaster, characterized by its complex and gradual onset. It affects more people than any other natural disaster and leads to severe economic, social, and environmental consequences [1,2]. According to the IPCC Sixth Assessment Report (AR6), global temperatures are expected to exceed a 1.5 °C increase from pre-industrial levels (1850–1900) within the next 20 years [3]. As global climate changes, rising surface temperatures and the urban heat island effect will lead to more frequent and severe agroecological droughts, impacting the sustainable development of soil environments and human activities[4–6]. Agriculture, as the cornerstone of the national economy, is crucial for food security and sustainable development. Therefore, real-time or near-real-time monitoring of agricultural drought serves as an effective measure in safeguarding the national economy.

Soil moisture plays a significant role in crop growth and development. Precise soil moisture data enables the accurate planning of irrigation schedules for crop growth, thereby promoting the advancement of modern agriculture [7,8]. While traditional surface soil

* Corresponding author.
E-mail addresses: wx2734747093@163.com (X. Wang), gislhx@hebeu.edu.cn (H. Liu).

https://doi.org/10.1016/j.heliyon.2024.e37426
Received 27 May 2024; Received in revised form 2 September 2024; Accepted 3 September 2024
Available online 4 September 2024

moisture measurement is highly accurate, it is limited by its point-based approach, small coverage area, and variability in soil depth [9,10]. The development of remote sensing technology offers new spatial solutions to numerous environmental problems, including forest fire risk, urban heat island effect, and land use relationships[11–13]. Satellite remote sensing has become essential for the timely detection and monitoring of drought, providing rapid access to global spatiotemporal data [14,15].

Over the years, both domestic and international researchers have extensively explored drought conditions and soil moisture using various remote sensing drought indices. Ahmed et al. [16] utilized the positive correlation between the normalized difference vegetation index (NDVI) and soil moisture to determine the optimal time lag in soil moisture changes, thereby addressing vegetation dynamics. Zhang et al. [17] used the surface water content index (SWCI) for monitoring shallow soil water, demonstrating its superior ability to depict surface water content values and changes compared to NDVI. Pathak et al. [18] analyzed a 13-year vegetation condition index (VCI) and the standardized soil moisture index, finding a strong correlation between them. Casamitjana et al. [19] employed drones to study the correlation between three types of agricultural land (potato, bare soil, and pasture) and surface soil moisture, identifying the normalized difference water index (NDWI) as particularly effective for monitoring bare soil, with a significant correlation specifically noted for potato cultivation. Zhang et al. [20] conducted an initial investigation on the normalized multi-band drought index (NMDI), revealing a significant correlation between NMDI and soil moisture at depths of 0–50 cm. Kukunuri et al. [21] integrated the vegetation condition index (VCI) and the temperature condition index (TCI), which reflect crop canopy temperature, to assess overall vegetation health for more accurate agricultural drought estimation. Yu et al. [22] emphasized the strong correlation between the vegetation supply water index (VSWI) and soil moisture during soil water inversion. Yuan et al. [23] developed a model that integrates the temperature vegetation dryness index (TVDI) and apparent thermal inertia (ATI) within the characteristic space of surface temperature and vegetation index to accurately represent soil moisture in the Loess Plateau. Li et al. [24] examined the spatial variation characteristics of agricultural drought using the TVDI system. However, different remote sensing drought indices vary in their sensitivity to vegetation coverage, leading to differing capabilities in drought monitoring depending on the context [25]. The GNSS navigation system is widely used due to its sensitivity to soil moisture, but its signal is easily disturbed and has certain limitations [26,27]. Soil moisture is a complex nonlinear coupling system, and a single drought index often fails to fully capture its dynamics. Consequently, the nonlinear integration of various drought monitoring parameters has increasingly become the focus of research [28].

With advancements in machine learning technology, powerful tools have emerged for managing dynamic and nonlinear systems. Machine learning algorithms, such as support vector machines (SVM), random forests (RF), and radial basis function neural networks (RBFNN), are widely applied in remote sensing[29–32]. Despite the strong performance of these models across various domains, Zhu et al. [33] found that artificial neural networks outperform RF and linear models in soil moisture estimation. Neural networks process information through mathematical methods, making them more susceptible to modal requirements compared to most parameter-based nonlinear methods [34]. Unlike RBFNN, backpropagation neural networks (BPNN) are prone to local minimum problems and have slow learning rates, which complicates their structure. Consequently, RBFNN is a suitable choice for nonlinear system identification [35,36]. Xie et al. [37] demonstrated that RBFNN effectively predicts the nonlinear relationship between soil moisture and environmental variables. Meanwhile, Hosseini-Moghari et al. [38] utilized the neural network method to demonstrate the significant advantages of RBF methods in predicting drought index values. Based on this, this study selects RBFNN as the primary model to fit the nonlinear relationship between different drought monitoring parameters, enabling the extrapolation of station-based soil moisture to regional scales and improving the accuracy of regional soil moisture inversion. The model of this study is easy to use and delivers results quickly, greatly improving efficiency. The main objectives of this study are: (1) capturing the complex interactions affecting soil moisture and constructing an optimal set of drought indices; (2) evaluating RBFNN's performance in fitting soil moisture;

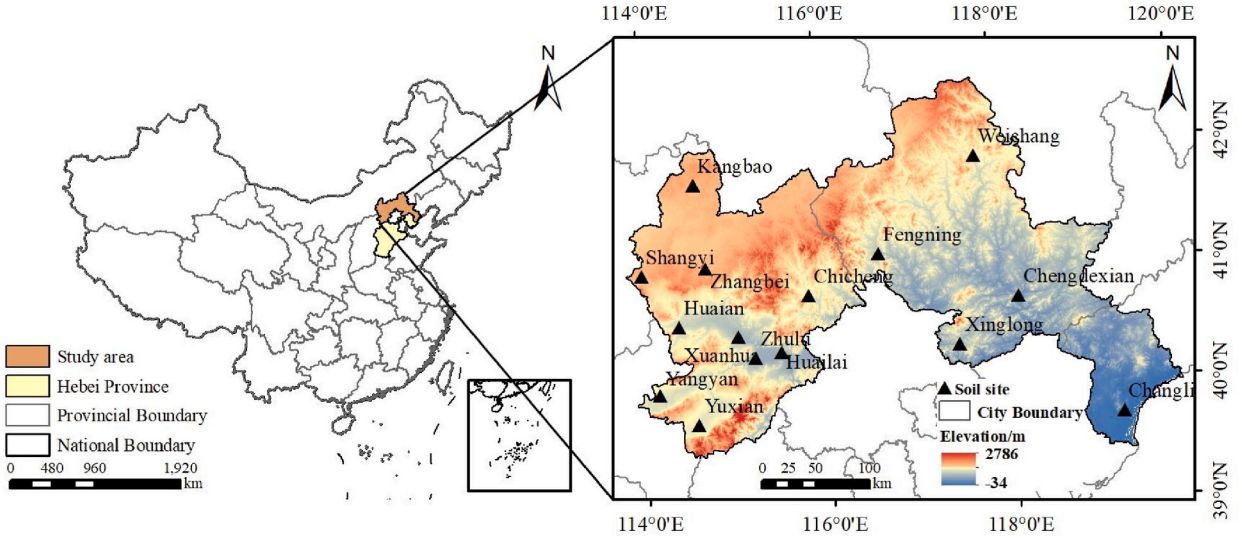

Fig. 1. Overview of the study area and distribution of soil moisture monitoring sites.

and (3) conducting large-scale soil moisture inversion for regional spatial scales. Through this study, the goal is to advance the application of different information factor modelling technologies and provide insights and references for agricultural drought monitoring.

2. Materials and methods

2.1. Study area

The study area encompasses the northern region of Hebei Province, specifically including Zhangjiakou City, Chengde City, and Qinhuangdao City. Situated in North China, this area spans from 113°27′E to 119°50′E longitude and 36°05′N to 42°40′N latitude. The landform is complex and diverse, primarily consisting of the plateau on the dam and the hilly mountain terrain beneath the dam (Fig. 1). The region features a temperate and warm temperate continental monsoon climate, characterized by seasonal precipitation and heat, as well as distinct four seasons. With approximately 2885 annual sunshine hours, the climate varies due to factors such as latitude, terrain, altitude, and atmospheric circulation. The dam area, influenced by northwest airflow, experiences predominantly dry, cold, and windy conditions year-round, with an average annual temperature of approximately 2 °C, a frost-free period of 87–126 days, annual precipitation of around 390 mm, and over 60 days of strong winds annually. Conversely, the mountainous and hilly areas have a more complex climate, with an average annual temperature of 7.6 °C, a frost-free period of 120–180 days, and annual precipitation totalling 450 mm. Rainfall is concentrated primarily from July to September, accounting for about 70 %–80 % of the total annual precipitation.

2.2. Data source and processing

2.2.1. Remote sensing data

Surface temperature data (MOD11A2) and surface reflectivity data (MOD09A1) used in this study were obtained from NASA's official website (https://www.nasa.gov/) for the period spanning July 2001 to 2013. The data cover the regions identified by the serial numbers H26V04, H26V05, H27V04, and H27V05. MOD11A2 is an 8-day composite product with a spatial resolution of 1 km, while MOD09A1 is also an 8-day composite with a higher spatial resolution of 500 m and includes information across 7 spectral bands. Following pre-processing using the MRT tool (including splicing and reprojection), MOD11A2 surface temperature data was resampled to 500 m to match the spatial resolution of MOD09A1 reflectivity data. This standardization facilitates the calculation of various drought indices. Data from the MOD11A2 image dated July 20 were excluded due to extensive missing pixels, as indicated in Table 1. The usage of MOD09A1 data followed a similar protocol to MOD11A2.

2.2.2. Soil relative humidity data

The China Meteorological Data website (http://data.cma.cn/) hosts a dataset on soil relative humidity, which provides observations at ten-day intervals. This dataset includes information relevant to crop growth, farmland soil moisture, and relative soil moisture at various depths, collected from soil moisture stations. For July 2012, 15 stations with complete data were selected within the study area (Fig. 1), while a total of 45 stations recorded observed data over three consecutive ten-day periods. The RBFNN model employed soil moisture data sampled at depths of 10 cm and 20 cm, referred to as SM10 and SM20, respectively.

2.2.3. Meteorological data

Meteorological data were obtained from the China Meteorological Data official website (http://data.cma.cn/). The dataset covers the period from 1950 to 2015 and encompasses crucial meteorological parameters, such as daily temperature and precipitation. Monthly average temperature and accumulated precipitation statistics were calculated from this data. Additionally, the precipitation anomaly percentage was calculated to facilitate further comparative analysis.

2.3. Methodology

2.3.1. Construction of MODIS drought index

Many researchers, both domestically and internationally, have investigated drought conditions and utilized observed soil moisture data for soil moisture inversion and drought monitoring[16–24]. This study has integrated multiple parameters, including crop canopy temperature, morphology, greenness, soil moisture, and canopy water content, to compile a dataset and identify eight key remote sensing drought indices such as SWCI, TCI, and TVDI. The computational equations for each index are delineated in Table 2.

Table 2 presents the MOD09A1 product band specifications as follows: b_1 (620–670 nm), b_2 (841–876 nm), b_4 (545–565 nm), b_6

Table 1
MOD11A2 image data.

Data source	Spatial resolution	Temporal resolution	Data number	Date	Ten-day
MOD11A2	1 km	8 days	185	7.04	first
			193	7.12	middle
			209	7.28	last

(1628–1652 nm), and b_7 (2105–2155 nm). Here, LST represents surface temperature, with LST_{max} and LST_{min} denoting the maximum and minimum values observed over multiple years within the same period. $NDVI_{max}$ and $NDVI_{min}$ indicate the highest and lowest NDVI values recorded during the corresponding timeframe. *LST(max)* and *LST(min)* refer to the maximum and minimum surface temperatures, respectively, with coefficients a_1, a_2, c_1, and c_2 denoting undetermined parameters.

The development of various factors and subsequent model construction is approached from the perspective of different drought monitoring parameters, as shown in Fig. 2.

2.3.2. Construction of RBFNN inversion model

The radial basis function neural network (RBFNN) is a feedforward artificial neural network renowned for its excellent performance, efficient modelling, rapid operation speed, and strong nonlinear mapping capabilities [47]. Structurally, the RBFNN is an advanced form of the multi-layer perceptron neural network (MLPNN), organized into three layers: input layer, hidden layer, and output layer. Each node (neuron) within the hidden layer serves as a processing unit, employing the RBF as its activation function within the MLPNN framework [34]. Fig. 3 illustrates the schematic diagram depicting the neural network topology.

The input layer of the RBFNN consists of a K-dimensional vector $X'_p = \{X'_{p1}, X'_{p2}, \ldots, X'_{pk}\}$, representing eight distinct indicators from remote sensing drought monitoring.

In the RBFNN's hidden layer, the activation function used is the radial basis function, commonly employing the Gaussian function due to its unique properties defined by centre and width parameters. The formula is as follows (1):

$$\phi(X', \sigma) = exp\left[\frac{-(X' - C_j)^2}{2\sigma_j^2}\right] \tag{1}$$

here, φ represents the Gaussian function, X' denotes the set of remote sensing drought monitoring indices, C_j indicates the centre of the kernel function for the j^{-th} hidden layer element, and σ_j stands for the width vector for the j^{-th} hidden layer element, determining the radial range of the function. The radial basis function measures the Euclidean distance between the input (X) and the centre (C_j), transforming it nonlinearly within the hidden layer [48].

The output layer of the RBFNN yields the relative soil moisture at various depths, specifically at soil moisture locations SM10 and SM20. The formula is as follows (2):

$$Y_j = \sum_{h=1}^{k} W_h \times f(X', \sigma) \tag{2}$$

Here, W represents the weight value and h denotes the number of output layers ($h = 1, 2, \ldots, k$).

The radial basis function is widely employed as an approximation function. Constructing an RBF network involves iterative adjustments, where neurons are incrementally added to the hidden layer until the network's output error reaches a predetermined RMSE. During this process, the following key parameters are continuously debugged to achieve the optimal results. The formula is as follows (3):

$$net = newrb(P, T, goal, spread, MN, DF) \tag{3}$$

here, *newrb* refers to the RBF function, *net* represents the returned RBF network object, P denotes the input sample vector of the network, T signifies the output target vector, *goal* stands for the RMSE goal, *spread* represents the spread rate of the RBF, *MN* indicates

Table 2
Drought monitoring parameters and algorithms for remote sensing drought indices.

Drought monitoring parameter	Remote sensing drought index	Index algorithm	Literature
Soil moisture content	SWCI	$SWCI = \frac{b_6 - b_7}{b_6 + b_7}$	[39]
	VSWI	$VSWI = \frac{NDVI}{LST}$	[40]
Crop morphology and greenness	NDVI	$NDVI = \frac{b_2 - b_1}{b_2 + b_1}$	[41]
	VCI	$VCI = \frac{NDVI - NDVI_{min}}{NDVI_{max} - NDVI_{min}}$	[42]
Crop canopy water content	NDWI	$NDWI = \frac{b_2 - b_4}{b_2 + b_4}$	[43]
	NMDI	$NMDI = \frac{b_2 - (b_6 - b_7)}{b_2 + (b_6 - b_7)}$	[44]
Crop canopy temperature	TCI	$TCI = \frac{LST_{max} - LST}{LST_{max} - LST_{min}}$	[45]
Characteristic space of surface temperature and vegetation index	TVDI	$TVDI = \frac{LST - LST(min)}{LST(max) - LST(min)}$ $LST(max) = a_1 + c_1 NDVI$ $LST(min) = a_2 + c_2 NDVI$	[46]

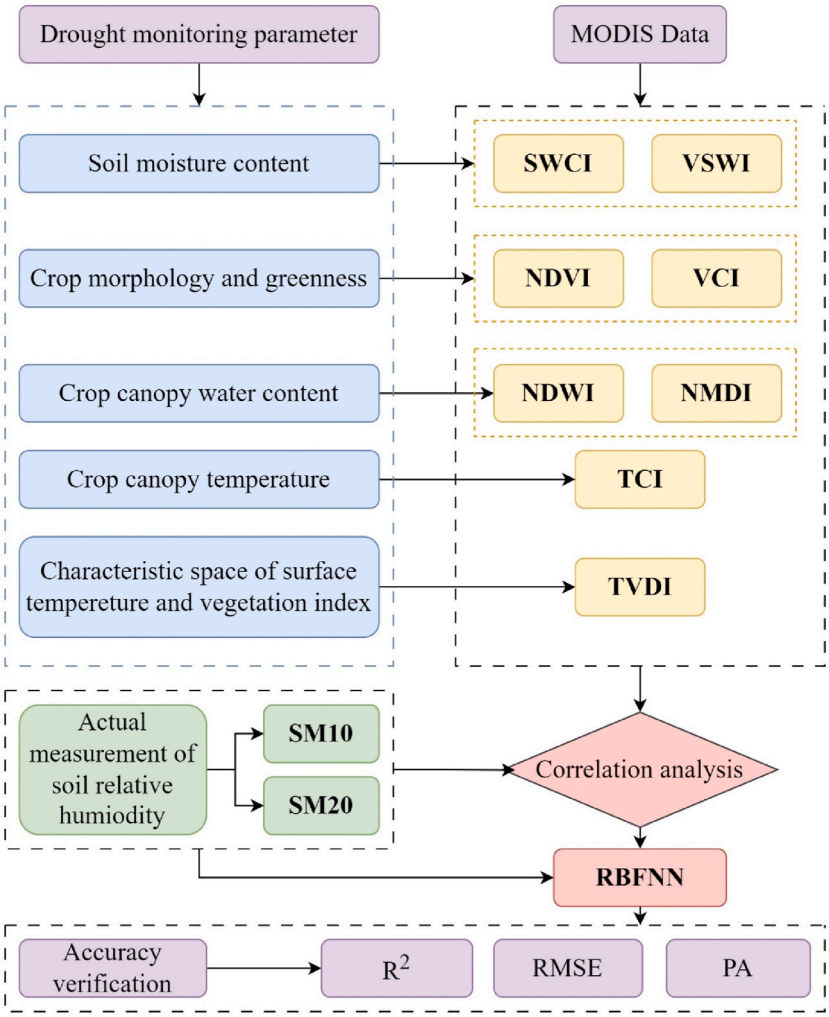

Fig. 2. Various indices and technical frameworks for developing RBFNN.

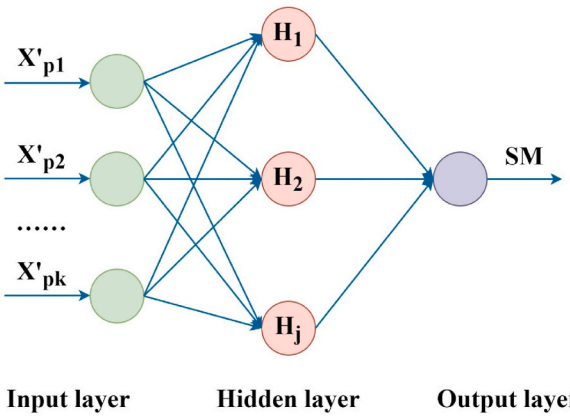

Fig. 3. Overview of the study area and distribution of soil moisture monitoring sites.

the maximum number of neurons, and *DF* denotes the number of neurons added between two display updates during training.

2.3.3. Correlation analysis

Correlation analysis examines the signs of casual relationships overall, describing the proximity between objective elements and using specific indicators for statistical purposes[49–51]. This study uses Pearson correlation analysis, which measures the degree of correlation between two variables [52]. By assessing correlations between eight remote sensing drought indices and measured soil moisture, optimal indices for different soil depths were identified. Furthermore, the study analyses the correlation between RBFNN inversion results and measured soil moisture.

The r is calculated as follows (4):

$$r = \frac{\sum_{i=1}^{n}(X_i - \overline{X})(Y_i - \overline{Y})}{\sqrt{\sum_{i=1}^{n}(X_i - \overline{X})^2}\sqrt{\sum_{i=1}^{n}(Y_i - \overline{Y})^2}} \tag{4}$$

here, $\overline{X}$ represents the average value of the X variable and $\overline{Y}$ represents the average value of the Y variable. The correlation coefficient r ranges between −1 and 1. A value of 1 indicates perfect positive correlation, −1 indicates perfect negative correlation, and 0 signifies no linear correlation.

2.3.4. Model accuracy verification method

In order to verify the precision and reliability of the soil relative humidity inversion model, several evaluation metrics were employed, including the coefficient of determination (R^2), root mean square error (RMSE), and inversion accuracy (PA). A higher R^2 indicates better model fitting while a smaller RMSE signifies greater accuracy, reflecting higher model quality. Conversely, lower values indicate poorer model performance.

The coefficient of determination is calculated as follows (5):

$$R^2 = 1 - \frac{\sum_{i=1}^{n}(X_i - Y_i)^2}{\sum_{i=1}^{n}(X_i - \overline{Y}_i)^2} \tag{5}$$

The root mean square error is calculated as follows (6):

$$RMSE = \sqrt{\frac{1}{n}\sum_{i=1}^{n}(X_i - Y_i)^2} \tag{6}$$

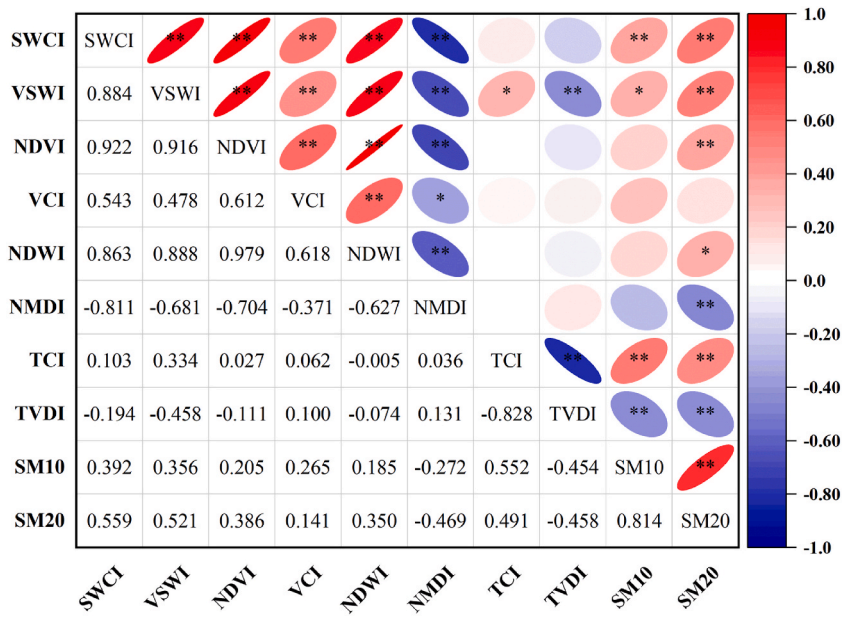

Fig. 4. Correlation heatmap of remote sensing drought monitoring indices and soil moisture. ** and * represent the 1 % and 5 % significance levels, respectively.

Inversion accuracy is calculated as follows (7):

$$PA = 1 - (|PV - MV|)/MV \times 100\% \quad (7)$$

Here, n represents the total number of samples, X_i and Y_i denote the i^{-th} measured and predicted values, respectively, indicating the average of the measured values, MV stands for measured value, PV signifies predicted value, and PA represents prediction accuracy in percentage.

3. Results

3.1. Optimal remote sensing drought index selection

Based on the remote sensing drought monitoring index algorithm outlined in Table 2, eight distinct remote sensing drought indices were calculated, and their correlation coefficients with SM10 and SM20 were determined. The heatmap displaying these correlation coefficients is shown in Fig. 4.

The correlation strengths between SM10 and the eight drought indices rank as follows: TCI > TVDI > SWCI > VSWI > NMDI > VCI > NDVI > NDWI. Similarly, for SM20, the correlation rankings with the eight drought indices are: SWCI > VSWI > TCI > NMDI > TVDI > NDVI > NDWI > VCI. Analysis of Fig. 4 indicates that TCI, reflecting crop canopy temperature, exhibits the strongest correlation with soil moisture at both depths, followed by SWCI and TVDI. These three indices, along with SM10 and SM20, all pass the 1 % significance test. VCI and TCI demonstrate stronger correlations with SM10, while the remaining 6 indices show stronger correlations with SM20, suggesting greater sensitivity of each index to soil water conditions at 20 cm depth. Therefore, the selection of remote sensing drought indices for soil moisture inversion varies by depth. SM20 achieves significance at the 1 % level with SWCI, VSWI, NDVI, NMDI, TCI, and TVDI, and at the 5 % level with NDWI. Consequently, these six indices (SWCI, VSWI, TCI, NMDI, TVDI, NDVI) passing the 1 % significance test were chosen as evaluation indices for the SM20 inversion model. In contrast, SM10 only passed the 1 % significance test with SWCI, TCI, and TVDI, while VSWI passed at the 5 % level. To maintain consistency in the number of remote sensing drought indices used for soil moisture inversion at different depths, the evaluation indices for the SM10 inversion model also included six indices (TCI, TVDI, SWCI, VSWI, NMDI, VCI).

3.2. Construction and accuracy evaluation of soil moisture inversion model

Data from 45 soil moisture sites in 2012 were randomly selected for analysis. A total of 36 groups (80 %) were used for training, while the remaining 9 groups (20 %) were used for testing, ensuring no overlap between the two sets. Prior to constructing the neural network model, the datasets were normalized and subjected to comprehensive performance testing. Predicted values from the test dataset underwent inverse normalization to calculate RMSE and PA. This process ensures the reliability of the neural network model across various datasets and provides robust performance metrics for subsequent data analysis. The test datasets SM10 and SM20 served as samples, with data from various sites and time periods within the test set (9 groups) used for validation to calculate their PA, as presented in Tables 3 and 4.

The soil moisture model, based on six MODIS drought indices and employing collaborative inversion with RBFNN, exhibits superior inversion effectiveness, as indicated in Tables 3 and 4. Specifically, the average inversion accuracy for SM10 and SM20 is 87.54 % and 87.36 %, respectively, accompanied by corresponding RMSE of 0.093 and 0.092 for the test set. These results clearly demonstrate the model's high-precision performance across two distinct soil layers, aligning with the model's robust performance in practical applications.

To further validate the impact of the RBFNN model on soil moisture inversion, a regression analysis was conducted using data from 45 sets of soil moisture sites to compare measured and predicted values. The analysis utilized correlation coefficient r, coefficient of determination R^2, and RMSE to assess the model's validity. Specifically, R^2 reflects the ratio of the total variation in the data explained by the model, serving as a crucial metric for assessing model fit. Meanwhile, RMSE is a standard measure for evaluating model performance, where lower values indicate higher accuracy and quality. The results of the regression analysis for SM10 and SM20 are depicted in Fig. 5.

The soil moisture model, developed through a combination of remote sensing drought indices and RBFNN, demonstrates clear

Table 3
Experimental results of SM10 soil moisture inversion model.

Site	Ten-day	Measured value/%	Predicted value/%	Prediction accuracy/%
Huaian	M	46.00	45.81	99.59
Yangyan	M	48.00	38.93	81.10
Yuxian	F	54.50	47.53	87.21
Weixian	M	49.50	63.90	70.91
Fengning	L	52.50	51.16	97.45
Weichang	F	43.00	48.26	87.77
Huailai	M	66.50	48.11	72.35
Xinglong	L	85.00	84.82	99.79
Changli	L	99.00	90.76	91.68

Table 4
Experimental results of SM20 soil moisture inversion model.

Site	Ten-day	Measured value/%	Predicted value/%	Prediction accuracy/%
Kangbao	L	77.00	79.74	96.44
Zhangbei	F	69.00	77.20	88.12
Zhangbei	L	60.00	63.99	93.35
Xuanhua	F	54.00	58.01	92.57
Xuanhua	L	58.00	68.59	81.74
Weichang	M	62.50	72.99	83.22
Huailai	L	74.67	65.22	87.34
Zhulu	L	66.00	82.03	75.71
Xinglong	F	75.00	65.80	87.73

Note: F represents the first ten days, M represents the middle ten days, and L represents the last ten days.

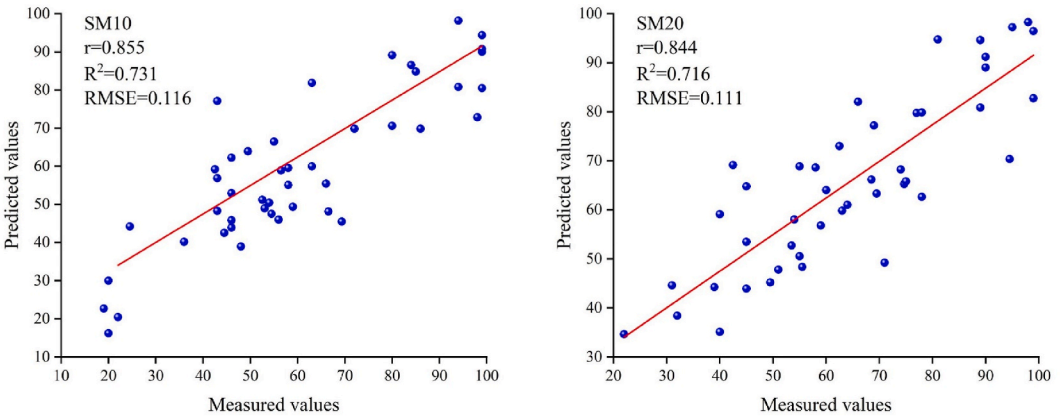

Fig. 5. Retrieval results of soil moisture in 2012.

superiority over using the six remote sensing drought indices individually for soil moisture retrieval. The measured values of SM10 and SM20 exhibited significant correlation with the predicted values, particularly for SM10, where the correlation coefficient (r) and determination coefficient (R^2) reached 0.855 and 0.731, respectively, indicating an excellent fit. Although SM20 showed slightly lower values than SM10, its correlation coefficient (r) and determination coefficient (R^2) were 0.844 and 0.716, respectively, indicating a satisfactory fit. The correlation between the two soil layers was similar, with both demonstrating positive outcomes. Furthermore, calculating the RMSE of the inversion results for the two soil layers revealed an RMSE of 0.111 for SM20 and 0.116 for SM10. This finding suggests that the prediction model accurately represents the experimental data and underscores its overall high quality. These results unequivocally demonstrate the outstanding performance of the soil moisture model constructed using remote sensing drought indices and RBFNN for accurate inversion.

3.3. Validity verification of soil moisture inversion model

To further validate the effectiveness of using drought indices and RBFNN for soil moisture retrieval, the study area was divided into 10 km resolution grids. The mean value method was employed to extract six remote sensing drought indices for each grid in 2013. Simultaneously, RBFNN successfully retrieved the 10 cm soil moisture values for three time periods (early, mid, and late) in July 2013. To obtain a more comprehensive distribution of soil relative humidity, the predicted values were interpolated using the Kriging method, resulting in maps depicting the distribution of 10 cm soil relative humidity across the study area for early, mid, and late July 2013 (Fig. 6).

Hebei Province is a significant agricultural region known for the extensive cultivation of spring corn in its northern part. This study focused on July to align with the jointing and flowering stages of spring maize. Soil moisture levels were classified according to the Northern Spring Maize Drought Grade (QXT 259–2015) [53], categorizing soil moisture (SM) levels as follows: SM $>$ 90 % as humid, 75 % $<$ SM $\leq$ 90 % as drought-free, 65 % $<$ SM $\leq$ 75 % as light drought, 55 % $<$ SM $\leq$ 65 % as medium drought, 45 % $<$ SM $\leq$ 55 % as severe drought, and SM $\leq$ 45 % as extreme drought. In Fig. 6, during the first ten days of the study year, Zhangjiakou exhibited severe, moderate, and light drought conditions, with some areas experiencing drought-free or humid conditions. Chengde City showed concentrated drought in the north, with moisture levels increasing from north to south, while drought in Qinhuangdao City was mainly confined to the southern region. During the middle phase of the study, drought conditions intensified in Zhangjiakou City, particularly in the northwest area where severe drought escalated to extreme levels, while the southern areas saw moderate drought expand. Conversely, Chengde City witnessed a reduction in drought-affected areas, with only a limited northern region experiencing moderate

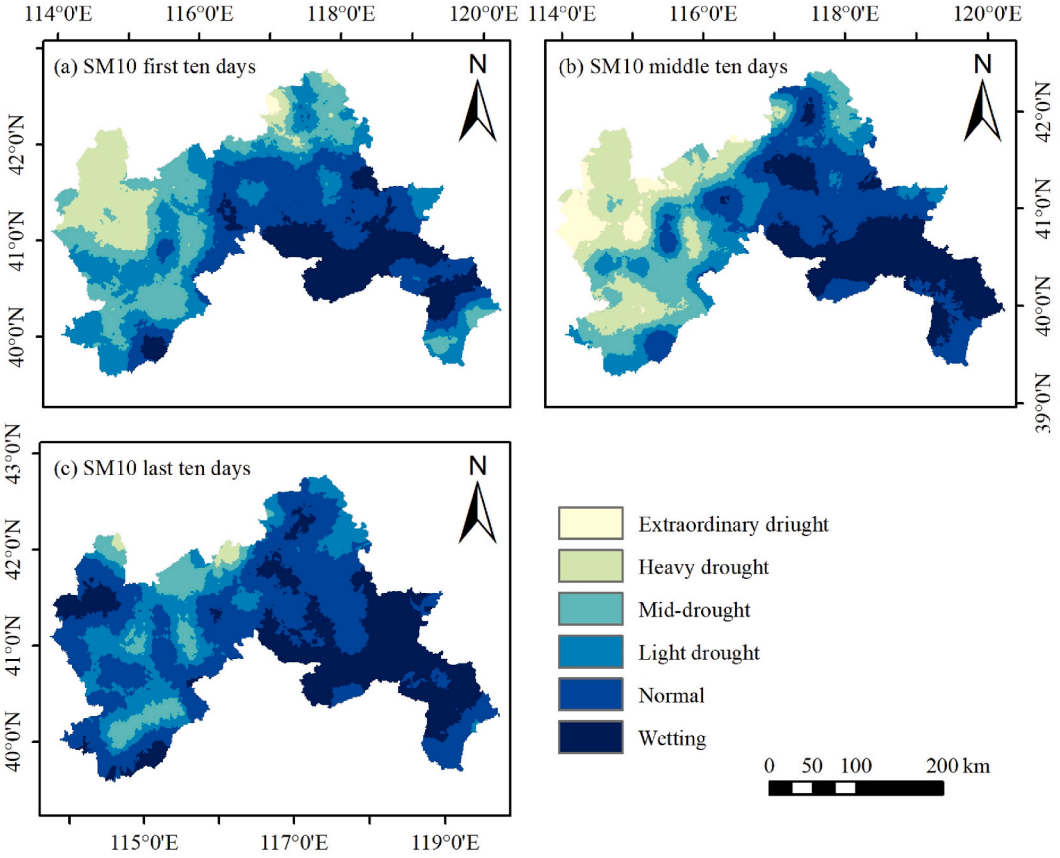

Fig. 6. RBFNN collaborative retrieval of soil relative humidity at a depth of 10 cm using remote sensing drought indices in July 2013.

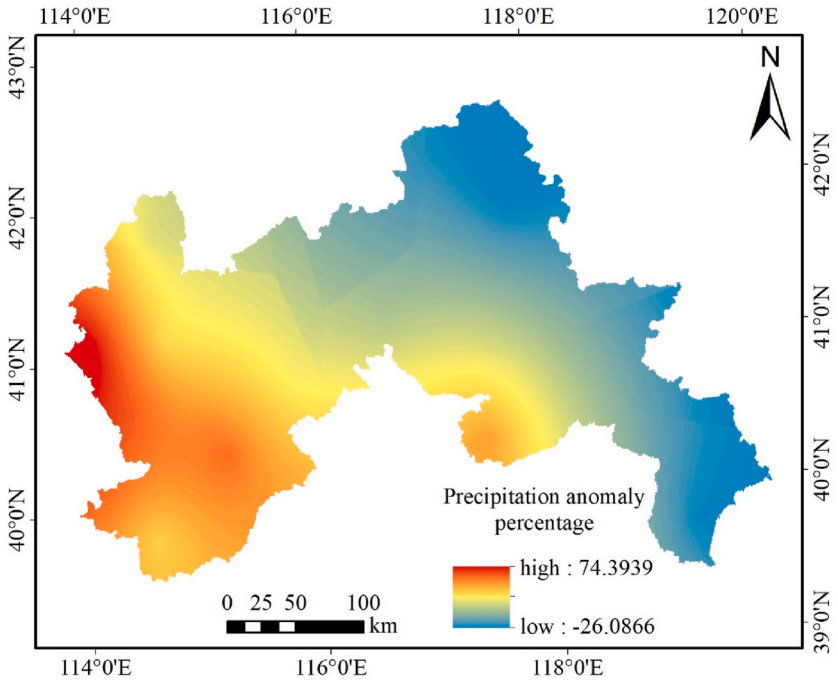

Fig. 7. Precipitation anomaly percentage in July 2013.

drought, and Qinhuangdao City remained largely unaffected by drought. Toward the end of the study period, the drought situation in the study area improved. In Zhangjiakou City, severe drought was limited to a few areas, with predominant occurrences of light drought and even some areas reaching a humid state. Chengde City's drought-affected area continued to shrink, while Qinhuangdao City remained free of drought. The inversion results effectively captured short-term regional changes in SM10, facilitating large-scale regional monitoring objectives.

Overall, the drought conditions in the study area exhibited a decreasing trend in July 2013, with a significant area experiencing no drought or even humid conditions, particularly noticeable in Zhangjiakou City. A comparison of the interpolated precipitation anomaly percentage based on meteorological station data from July 2013 (Fig. 7) revealed that overall precipitation levels in the study area surpassed the typical levels. The exceptions were the northern parts of Chengde City and Qinhuangdao City, where precipitation was lower, though not sufficiently low to trigger drought conditions based on the anomaly data. Moreover, according to the climate assessment bulletin from the Hebei Meteorological Bureau, the meteorological drought in Hebei Province in 2013 mainly occurred in spring and autumn due to continuous rainfall. The majority of this rainfall occurred from late June to mid-July, preventing severe drought conditions in the study area throughout July. These findings align with the model's predicted results, affirming the effectiveness of the inversion model in estimating soil moisture and further emphasizing its practical reliability. This study retrieved soil relative humidity for the first, middle, and last ten days of July, revealing that the overall drought situation alleviated from the beginning to the end of the month, eventually reaching a drought-free state. However, our inversion results indicate that there was an aggravation of drought conditions in certain areas of Zhangjiakou from early to mid-July. This suggests that soil relative humidity in these areas was not solely influenced by precipitation during this period. Other drought-causing factors played a significant role. Capturing this information is crucial for effective soil moisture monitoring. Detailed capture of soil moisture dynamics can contribute to the sustainable development of soil health and ensure optimal conditions for crop growth. At the same time, using more precise daily-scale data in the model would enhance the efficiency of capturing soil moisture changes, providing a more reliable reference for regional soil management and drought prevention.

4. Discussion

When selecting drought indicators, it is crucial to consider their impact on drought events. This study utilizes drought monitoring parameters from four different perspectives to ensure a comprehensive assessment of drought conditions during collaborative inversion. The selection process includes TVDI, which is based on surface temperature and vegetation index. Although previous studies have applied TVDI independently to monitor agricultural drought [54], it is not a direct parameter for characterizing soil information. This study aims to construct a drought index set by incorporating TVDI alongside indices representing various parameters. Correlation analysis shows that TVDI has a significant relationship with soil moisture, leading to notable results in subsequent inversions. Among the eight drought indices, TCI shows a significantly stronger correlation with soil relative humidity than other indices. This is primarily because TCI is highly sensitive to drought during dry seasons or high-temperature months [55]. Given that the study period is in July, TCI shows a significant correlation with soil relative humidity. In contrast, NDVI, VCI, and NDWI show a lower correlation with soil relative humidity, likely due to influences from vegetation, soil type, terrain, and atmospheric conditions. Furthermore, these three indices exhibit time lag issues [56], further complicating their effectiveness in drought monitoring.

Soil moisture is influenced by a variety of factors. Precipitation, the primary component of the water balance, directly affects soil moisture levels. Temperature, by regulating evapotranspiration, indirectly impacts soil moisture [57]. Thus, soil moisture is largely a result of the balance between precipitation and evaporation [58,59]. The study demonstrates a correlation between the percentage of precipitation anomaly and the inversion of SM10 in 2013. In addition, a comparative analysis of temperature and precipitation data from various stations in 2012 (Fig. 8) indicates that soil moisture trends at each station align with precipitation trends, while temperature-influenced fluctuations in soil moisture are relatively minor. Despite the significant impact of precipitation, the inversion results effectively capture droughts caused by non-precipitation factors, highlighting the model's effectiveness. Moreover, factors such as elevation, slope, land type, and other site-specific characteristics also influence soil moisture. Consequently, future research should include long-term analysis and a comprehensive discussion that integrates elevation, slope, land type, evapotranspiration, and human influences. This comprehensive approach will provide a deeper understanding of the factors driving soil moisture changes, enhance predictive capabilities and responses to drought events, and provide a more accurate scientific reference for managing agricultural water resources.

Advancements in machine learning technology have led to its extensive application across various industries and fields. One of its key strengths is its ability to handle noisy data from dynamic and nonlinear systems without requiring an extensive dataset [60,61]. For example, Zhang et al. [62] utilized RBFNN inversion to achieve an R^2 of 0.611 in retrieving winter wheat farmland surface soil moisture through machine learning. In this study, the inversion accuracy for SM10 ($R^2 = 0.731$) is slightly higher, likely due to the correlation of the selected drought parameters. Moreover, the study demonstrates certain advantages within the permissible error range due to regional discrepancies. The model's accuracy in soil moisture inversion exceeds 85 %, outperforming other monitoring methods [63,64]. As a result, regional soil moisture inversion can be effectively achieved using neural network models combined with various drought index models. The northern part of Hebei Province, a crucial grain production area in northern China, experiences sparse precipitation and frequent droughts [65]. Using a drought index set to retrieve soil moisture and monitor its dynamic changes across a large area is vital for disaster prevention, mitigation, and ensuring food security. At the same time, this method provides scientific support for the application and refinement of the RBFNN model in Hebei Province and serves as a case reference for regional soil moisture inversion.

Finally, it is important to acknowledge some limitations of this study. First, the training samples for soil moisture are limited by the

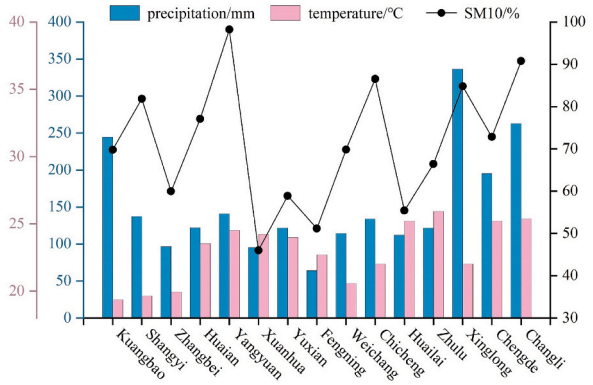

Fig. 8. Comparison of SM10 with temperature and precipitation at various stations in 2012.

number of soil moisture sites in the study area, which limits their representativeness. Second, there are some errors due to discrepancies between the measured data and the remote sensing area data. In addition, the study only considers optical remote sensing data when selecting model variables. Currently, multi-band microwave remote sensing information shows great potential for improvement [66]. Future research should incorporate microwave drought indices into the index set to retrieve more comprehensive multi-band remote sensing information.

5. Conclusions

This study focuses on the northern part of Hebei Province, where a remote sensing drought index is developed based on MODIS data, and soil moisture inversion is explored using RBFNN. The conclusions are as follows.

1) By analysing the correlation between remote sensing drought monitoring indices and soil relative humidity at different depths, TCI, TVDI, SWCI, VSWI, NMDI, and VCI were selected for the SM10 inversion model, while SWCI, VSWI, TCI, NMDI, TVDI, and NDVI were chosen for the SM20 model. This comprehensive index selection aims to accurately capture dynamic changes in soil moisture and provide reference indices for soil moisture inversion in northern Hebei Province.
2) The soil moisture retrieval model based on collaborative RBFNN significantly outperforms the six individual remote sensing drought indices. The correlations for SM10 ($r = 0.855$, $R^2 = 0.731$) and SM20 ($r = 0.844$, $R^2 = 0.716$) with measured soil moisture are strong, achieving retrieval accuracy of over 87 %. This greatly improves soil moisture retrieval accuracy in northern Hebei Province.
3) Using 2013 as a case study, the grid method enables large-scale regional soil moisture inversion. The results were consistent with the actual conditions and successfully detected dynamic changes in soil moisture caused by abnormal factors, further confirming the method's effectiveness and practicability.

Funding statement

This study was supported by National Natural Science Foundation of China (42071246, 42171212), and HeBei Provincial Natural Science Foundation of China (E2020402006, E2020402086, D2022402030).

Data availability statement

The data presented in this study are available on request from the first author. The data are not publicly available due to privacy.

Ethics statement

Review or approval by an ethics committee was not needed for this study because no data on patients or experimental animals was used in the article. Informed consent was not required for this study because no clinical data was produced in the reaserch article.

CRediT authorship contribution statement

Xiao Wang: Writing – review & editing, Writing – original draft, Visualization, Validation, Software, Resources, Methodology, Investigation. **Haixin Liu:** Writing – review & editing, Supervision, Project administration, Funding acquisition, Formal analysis, Data curation. **Zhenyu Sun:** Writing – original draft, Visualization, Supervision, Conceptualization. **Xiaoqing Han:** Supervision, Project administration, Funding acquisition.

Declaration of competing interest

The authors declare the following financial interests/personal relationships which may be considered as potential competing interests:The author declare that they have no known competing financial interest or personal relationships that could have appeared to influence the work reported in this paper. If there are other authors, they declare that they have no known competing financial interests or personal relationships that could have appeared to influence the work reported in this paper.

References

[1] A.-A. Belal, H.R. El-Ramady, E.S. Mohamed, A.M. Saleh, Drought risk assessment using remote sensing and GIS techniques, Arabian J. Geosci. 7 (2014) 35–53, https://doi.org/10.1007/s12517-012-0707-2.

[2] J. Li, Y. Li, L. Yin, Q. Zhao, A novel composite drought index combining precipitation, temperature and evapotranspiration used for drought monitoring in the Huang-Huai-Hai Plain, Agric. Water Manag. 291 (2024) 108626, https://doi.org/10.1016/j.agwat.2023.108626.

[3] T. Zhou, New physical science behind climate change: what does IPCC AR6 tell us? Innovation 2 (2021) https://doi.org/10.1016/j.xinn.2021.100173.

[4] I. Zeren Cetin, T. Varol, H.B. Ozel, A geographic information systems and remote sensing–based approach to assess urban micro-climate change and its impact on human health in Bartin, Turkey, Environ. Monit. Assess. 195 (2023) 540, https://doi.org/10.1007/s10661-023-11105-z.

[5] M. Cetin, F. Adiguzel, Ilknur zeren cetin, determination of the effect of urban forests and other green areas on surface temperature in antalya, in: M.N. Suratman (Ed.), Concepts and Applications of Remote Sensing in Forestry, Springer Nature, Singapore, 2022, pp. 319–336, https://doi.org/10.1007/978-981-19-4200-6_16.

[6] B. Degerli, M. Çetin, Evaluation from rural to urban scale for the effect of NDVI-NDBI indices on land surface temperature, Samsun, Türkiye, Turkish Journal of Agriculture - Food Science and Technology 10 (2022) 2446–2452, https://doi.org/10.24925/turjaf.v10i12.2446-2452.5535.

[7] D.G. Miralles, A.J. Teuling, C.C. van Heerwaarden, J. Vilà-Guerau de Arellano, Mega-heatwave temperatures due to combined soil desiccation and atmospheric heat accumulation, Nat. Geosci. 7 (2014) 345–349, https://doi.org/10.1038/ngeo2141.

[8] S. Chatterjee, A.R. Desai, J. Zhu, P.A. Townsend, J. Huang, Soil moisture as an essential component for delineating and forecasting agricultural rather than meteorological drought, Rem. Sens. Environ. 269 (2022) 112833, https://doi.org/10.1016/j.rse.2021.112833.

[9] W. Song, Y. Lu, Y. Wang, J. Lu, H. Shi, A pixel-scale measurement method of soil moisture using ground-penetrating radar, Water 15 (2023) 1318, https://doi.org/10.3390/w15071318.

[10] Q. Cheng, Q. Su, A. Binley, J. Liu, Z. Zhang, X. Chen, Estimation of surface soil moisture by a multi-elevation UAV-based ground penetrating radar, Water Resour. Res. 59 (2023) e2022WR032621, https://doi.org/10.1029/2022WR032621.

[11] M. Cetin, M. Ozenen Kavlak, M.A. Senyel Kurkcuoglu, G. Bilge Ozturk, S.N. Cabuk, A. Cabuk, Determination of land surface temperature and urban heat island effects with remote sensing capabilities: the case of Kayseri, Türkiye, Nat. Hazards 120 (2024) 5509–5536, https://doi.org/10.1007/s11069-024-06431-5.

[12] M. Cetin, Ö. Isik Pekkan, M. Ozenen Kavlak, I. Atmaca, S. Nasery, M. Derakhshandeh, S.N. Cabuk, GIS-based forest fire risk determination for Milas district, Turkey, Nat. Hazards 119 (2023) 2299–2320, https://doi.org/10.1007/s11069-022-05601-7.

[13] I. Zeren Cetin, H. Sevik, Investigation of the relationship between bioclimatic comfort and land use by using GIS and RS techniques in Trabzon, Environ. Monit. Assess. 192 (2020) 71, https://doi.org/10.1007/s10661-019-8029-4.

[14] W. Jiao, L. Wang, M.F. McCabe, Multi-sensor remote sensing for drought characterization: current status, opportunities and a roadmap for the future, Rem. Sens. Environ. 256 (2021) 112313, https://doi.org/10.1016/j.rse.2021.112313.

[15] M.W. Rasheed, J. Tang, A. Sarwar, S. Shah, N. Saddique, M.U. Khan, M. Imran Khan, S. Nawaz, R.R. Shamshiri, M. Aziz, M. Sultan, Soil moisture measuring techniques and factors affecting the moisture dynamics: a comprehensive review, Sustainability 14 (2022) 11538, https://doi.org/10.3390/su141811538.

[16] M. Ahmed, B. Else, L. Eklundh, J. Ardö, J. Seaquist, Dynamic response of NDVI to soil moisture variations during different hydrological regimes in the Sahel region, Int. J. Rem. Sens. 38 (2017) 5408–5429, https://doi.org/10.1080/01431161.2017.1339920.

[17] H. Zhang, H. Chen, R. Sun, W. Yu, C. Zou, S. Shen, The Application of Unified Surface Water Capacity Method in Drought Remote Sensing Monitoring, vol. 7472, 2009, https://doi.org/10.1117/12.829735.

[18] A. Pathak, B. Dodamani, Application of Remotely Sensed NDVI and Soil Moisture to Monitor Long-Term Agricultural Drought, 2019, p. 42, https://doi.org/10.1117/12.2532852.

[19] M. Casamitjana, M.C. Torres-Madroñero, J. Bernal-Riobo, D. Varga, Soil moisture analysis by means of multispectral images according to land use and spatial resolution on andosols in the Colombian andes, Appl. Sci. 10 (2020) 5540, https://doi.org/10.3390/app10165540.

[20] H. Zhang, H.-L. Chen, S. Shen, in: C.M.U. Neale, A. Maltese (Eds.), The Application of Normalized Multi-Band Drought Index (NMDI) Method in Cropland Drought Monitoring, 2009, p. 74721Q, https://doi.org/10.1117/12.830557. Berlin, Germany.

[21] A. Kukunuri, D. Murugan, D. Singh, Variance based fusion of VCI and TCI for efficient classification of agriculture drought using MODIS data, Geocarto Int. 37 (2020) 1–22, https://doi.org/10.1080/10106049.2020.1837256.

[22] Y. Yu, J. Wang, F. Cheng, Y. Chen, Soil moisture by remote sensing retrieval in the tropic of cancer of yunnan Province, Pol. J. Environ. Stud. 29 (2020), https://doi.org/10.15244/pjoes/110203.

[23] L. Yuan, L. Li, T. Zhang, L. Chen, J. Zhao, S. Hu, L. Cheng, W. Liu, Soil moisture estimation for the Chinese loess plateau using MODIS-derived ATI and TVDI, Rem. Sens. 12 (2020) 3040, https://doi.org/10.3390/rs12183040.

[24] Y. Li, X. Wang, F. Wang, K. Feng, H. Li, Y. Han, S. Chen, Temporal and spatial characteristics of agricultural drought based on the TVDI in henan Province, China, Water 16 (2024) 1010, https://doi.org/10.3390/w16071010.

[25] J. Wang, Y. Wang, L. Wang, Study on drought monitoring method of Liaoning Province based on FY-3D satellite, in: International Conference on Geographic Information and Remote Sensing Technology (GIRST 2022), 2023, pp. 639–645, https://doi.org/10.1117/12.2667446. SPIE.

[26] Y. Li, M. Zhu, L. Luo, S. Wang, C. Chen, Z. Zhang, Y. Yao, X. Hu, GNSS-IR dual-frequency data fusion for soil moisture inversion based on Helmert variance component estimation, J. Hydrol. 631 (2024) 130752, https://doi.org/10.1016/j.jhydrol.2024.130752.

[27] C. Yang, K. Mao, Z. Guo, J. Shi, S.M. Bateni, Z. Yuan, Review of GNSS-R technology for soil moisture inversion, Rem. Sens. 16 (2024) 1193, https://doi.org/10.3390/rs16071193.

[28] M.H. Jahangir, M. Arast, Estimation of surface soil moisture based on improved multi-index models and surface energy balance system, Nat. Resour. Res. 30 (2021) 789–804, https://doi.org/10.1007/s11053-020-09728-x.

[29] Z. Tang, W. Zhang, Y. Xiang, X. Liu, X. Wang, H. Shi, Z. Li, F. Zhang, Monitoring of soil moisture content of winter oilseed rape (Brassica napus L.) based on hyperspectral and machine learning models, J. Soil Sci. Plant Nutr. 24 (2024) 1250–1260, https://doi.org/10.1007/s42729-024-01626-y.

[30] Y. He, Z. Gong, Y. Zheng, Y. Zhang, Inland reservoir water quality inversion and eutrophication evaluation using BP neural network and remote sensing imagery: a case study of dashahe reservoir, Water 13 (2021) 2844, https://doi.org/10.3390/w13202844.

[31] C. Xiujia, Y. Guanghua, G. Jian, M. Ningning, W. Zihao, Application of WNN-PSO model in drought prediction at crop growth stages: a case study of spring maize in semi-arid regions of northern China, Comput. Electron. Agric. 199 (2022) 107155, https://doi.org/10.1016/j.compag.2022.107155.

[32] M. Mokhtarzad, F. Eskandari, N. Jamshidi Vanjani, A. Arabasadi, Drought forecasting by ANN, ANFIS, and SVM and comparison of the models, Environ. Earth Sci. 76 (2017) 729, https://doi.org/10.1007/s12665-017-7064-0.

[33] Z. Zhu, C. Zhao, X. Jia, J. Wang, M. Shao, Prediction of deep soil water content (0–5 m) with in-situ and remote sensing data, Catena 222 (2023) 106852, https://doi.org/10.1016/j.catena.2022.106852.

[34] A.H. Kamel, H.A. Afan, M. Sherif, A.N. Ahmed, A. El-Shafie, RBFNN versus GRNN modeling approach for sub-surface evaporation rate prediction in arid region, Sustainable Computing: Informatics and Systems 30 (2021) 100514, https://doi.org/10.1016/j.suscom.2021.100514.

[35] D. Zhou, Analysis and research on nonlinear complex function approximation problem based on deep learning, scientific programming 2022. https://doi.org/10.1155/2022/6559868, 2022.
[36] H. Yu, T. Chen, Valid RBFNN adaptive control for nonlinear systems with unmatched uncertainties, IEEE Transact. Neural Networks Learn. Syst. (2023) 1–14, https://doi.org/10.1109/TNNLS.2023.3292115.
[37] B. Xie, X. Jia, Z. Qin, C. Zhao, M. Shao, Comparison of interpolation methods for soil moisture prediction on China's Loess Plateau, Vadose Zone J. 19 (2020) e20025, https://doi.org/10.1002/vzj2.20025.
[38] S.M. Hosseini-Moghari, S. Araghinejad, Monthly and seasonal drought forecasting using statistical neural networks, Environ. Earth Sci. 74 (2015) 397–412, https://doi.org/10.1007/s12665-015-4047-x.
[39] Z. Hong, W. Zhang, C. Yu, D. Zhang, L. Li, L. Meng, SWCTI: surface water content temperature index for assessment of surface soil moisture status, Sensors 18 (2018) 2875, https://doi.org/10.3390/s18092875.
[40] B.H. Trisasongko, D.R. Panuju, D. Shiddiq, L.O.S. Iman, R.I. Sholihah, S. Kusdaryanto, Constraints of VSWI in the estimation of drought extent using landsat data: a case of tuban, Indonesia, Procedia Environmental Sciences 24 (2015) 25–28, https://doi.org/10.1016/j.proenv.2015.03.004.
[41] P.P. Patil, M.P. Jagtap, N. Khatri, H. Madan, A.A. Vadduri, T. Patodia, Exploration and advancement of NDDI leveraging NDVI and NDWI in Indian semi-arid regions: a remote sensing-based study, Case Studies in Chemical and Environmental Engineering 9 (2024) 100573, https://doi.org/10.1016/j.cscee.2023.100573.
[42] F.N. Kogan, Droughts of the late 1980s in the United States as derived from NOAA polar-orbiting satellite data, Bull. Am. Meteorol. Soc. 76 (1995) 655–668, https://doi.org/10.1175/1520-0477(1995)076<0655:DOTLIT>2.0.CO, 2.
[43] B. Gao, NDWI—a normalized difference water index for remote sensing of vegetation liquid water from space, Rem. Sens. Environ. 58 (1996) 257–266, https://doi.org/10.1016/S0034-4257(96)00067-3.
[44] L. Wang, J.J. Qu, NMDI: a normalized multi-band drought index for monitoring soil and vegetation moisture with satellite remote sensing, Geophys. Res. Lett. 34 (2007), https://doi.org/10.1029/2007GL031021.
[45] F.N. Kogan, Application of vegetation index and brightness temperature for drought detection, Adv. Space Res. 15 (1995) 91–100, https://doi.org/10.1016/0273-1177(95)00079-T.
[46] I. Sandholt, K. Rasmussen, J. Andersen, A simple interpretation of the surface temperature/vegetation index space for assessment of surface moisture status, Rem. Sens. Environ. 79 (2002) 213–224, https://doi.org/10.1016/S0034-4257(01)00274-7.
[47] R. Lin, Z. Wei, R. Hu, H. Chen, Y. Li, B. Zhang, F. Wang, D. Hu, Construction and validation of surface soil moisture inversion model based on remote sensing and neural network, Atmosphere 15 (2024) 647, https://doi.org/10.3390/atmos15060647.
[48] F.A. Ruslan, A.M. Samad, Z.M. Zain, R. Adnan, Modelling flood prediction using Radial Basis Function Neural Network (RBFNN) and inverse model: a comparative study, in: 2013 IEEE International Conference on Control System, Computing and Engineering, 2013, pp. 577–581, https://doi.org/10.1109/ICCSCE.2013.6720031.
[49] A.N.R. Irawan, D. Komori, V.S.A. Hendrawan, Correlation analysis of agricultural drought risk on wet farming crop and meteorological drought index in the tropical-humid region, Theor. Appl. Climatol. 153 (2023) 227–240, https://doi.org/10.1007/s00704-023-04461-w.
[50] Y. Liu, F. Shan, H. Yue, X. Wang, Y. Fan, Global analysis of the correlation and propagation among meteorological, agricultural, surface water, and groundwater droughts, J. Environ. Manag. 333 (2023) 117460, https://doi.org/10.1016/j.jenvman.2023.117460.
[51] J. Wu, Y. Gu, K. Sun, N. Wang, H. Shen, Y. Wang, X. Ma, Correlation of climate change and human activities with agricultural drought and its impact on the net primary production of winter wheat, J. Hydrol. 620 (2023) 129504, https://doi.org/10.1016/j.jhydrol.2023.129504.
[52] S. Jalayer, A. Sharifi, D. Abbasi-Moghadam, A. Tariq, S. Qin, Assessment of spatiotemporal characteristic of droughts using in situ and remote sensing-based drought indices, IEEE J. Sel. Top. Appl. Earth Obs. Rem. Sens. 16 (2023) 1483–1502, https://doi.org/10.1109/JSTARS.2023.3237380.
[53] M.U. Jia, S.H.I. Xue-jia, J. Meng-jiao, W.U. Di, L.I.U. Yan-yan, Dynamic early warning model of maize drought grade based on bayes discriminant in jilin Province, Chin. J. Agrometeorol. 44 (2023) 410, https://doi.org/10.3969/j.issn.1000-6362.2023.05.006.
[54] W. Wan, Z. Liu, K. Li, G. Wang, H. Wu, Q. Wang, Drought monitoring of the maize planting areas in Northeast and North China Plain, Agric. Water Manag. 245 (2021) 106636, https://doi.org/10.1016/j.agwat.2020.106636.
[55] L.F. Amalo, R. Hidayat, Haris, comparison between remote-sensing-based drought indices in east java, IOP Conf. Ser. Earth Environ. Sci. 54 (2017) 012009, https://doi.org/10.1088/1755-1315/54/1/012009.
[56] H. Hamarash, A. Rasul, R. Hamad, A review of methods used to monitor and predict droughts. https://doi.org/10.20944/preprints202208.0539.v1, 2022.
[57] M. Koukoula, C.S. Schwartz, E.I. Nikolopoulos, E.N. Anagnostou, Understanding the impact of soil moisture on precipitation under different climate and meteorological conditions: a numerical sensitivity study over the CONUS, J. Geophys. Res. Atmos. 126 (2021) e2021JD035096, https://doi.org/10.1029/2021JD035096.
[58] H. Gardiya Weligamage, K. Fowler, T.J. Peterson, M. Saft, M.C. Peel, D. Ryu, Partitioning of precipitation into terrestrial water balance components under a drying climate, Water Resour. Res. 59 (2023) e2022WR033538, https://doi.org/10.1029/2022WR033538.
[59] S. Schulz, R. Becker, J.C. Richard-Cerda, M. Usman, T. aus der Beek, R. Merz, C. Schüth, Estimating water balance components in irrigated agriculture using a combined approach of soil moisture and energy balance monitoring, and numerical modelling, Hydrol. Process. 35 (2021) e14077, https://doi.org/10.1002/hyp.14077.
[60] K. Linka, A. Schäfer, X. Meng, Z. Zou, G.E. Karniadakis, E. Kuhl, Bayesian physics informed neural networks for real-world nonlinear dynamical systems, Comput. Methods Appl. Mech. Eng. 402 (2022) 115346, https://doi.org/10.1016/j.cma.2022.115346.
[61] Z. Wu, D. Rincon, J. Luo, P.D. Christofides, Handling noisy data in machine learning modeling and predictive control of nonlinear processes, in: 2021 American Control Conference (ACC), 2021, pp. 3345–3351, https://doi.org/10.23919/ACC50511.2021.9483103.
[62] C. Zhang, J. Zhao, L. Min, N. Li, Cooperative inversion of winter wheat covered surface soil moisture by multi-source remote sensing, in: IGARSS 2022 - 2022 IEEE International Geoscience and Remote Sensing Symposium, 2022, pp. 4192–4195, https://doi.org/10.1109/IGARSS46834.2022.9883903.
[63] S. Li, X. Xu, STUDY ON REMOTE SENSING MONITORING MODEL OF AGRICULTURAL DROUGHT BASED ON RANDOM FOREST DEVIATION CORRECTION, INMATEH, 2021, pp. 413–422, https://doi.org/10.35633/inmateh-64-41.
[64] R. Shen, A. Huang, B. Li, J. Guo, Construction of a drought monitoring model using deep learning based on multi-source remote sensing data, Int. J. Appl. Earth Obs. Geoinf. 79 (2019) 48–57, https://doi.org/10.1016/j.jag.2019.03.006.
[65] Q. Li, L. Chen, Y. Xu, Drought risk and water resources assessment in the Beijing-Tianjin-Hebei region, China, Sci. Total Environ. 832 (2022) 154915, https://doi.org/10.1016/j.scitotenv.2022.154915.
[66] J. Zhao, C. Zhang, L. Min, Z. Guo, N. Li, Retrieval of farmland surface soil moisture based on feature optimization and machine learning, Rem. Sens. 14 (2022) 5102, https://doi.org/10.3390/rs14205102.